# Organometal Trihalide Perovskite Single Crystals: A Next Wave of Materials for 25% Efficiency Photovoltaics and Applications Beyond?

Jinsong Huang,* Yuchuan Shao, and Qingfeng Dong

Department of Mechanical and Materials Engineering, and Nebraska Center for Materials and Nanoscience, University of Nebraska—Lincoln, Lincoln, Nebraska 68588-0656, United States

ABSTRACT: Hybrid perovskite single crystals have been recently revealed to have superior optoelectronic properties to perovskite polycrystalline thin films, especially the extraordinarily long carrier diffusion length due to the eliminated grain boundaries. One question that naturally arises is whether the single crystal hybrid perovskites can be a next wave of photoactive materials for even higher-efficiency devices. This Perspective presents an overview of the historic evolution in understanding of carrier diffusion length in $CH_3NH_3PbI_3$, the initial investigations of the synthesis of single crystalline hybrid perovskites, and the characterization of their optoelectronic properties. Our analysis indicates that single crystalline perovskite materials have potential to further boost photovoltaic device power conversion efficiency to 25%. The potential opportunities for the fundamental study of the perovskite intrinsic properties, particularly the carrier mobility and carrier recombination lifetime, and other fields such as radiation detectors are also briefed.
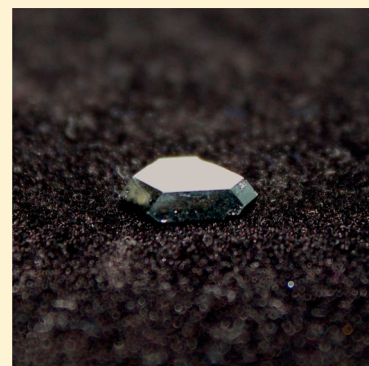
When it comes to solar cells, single-crystalline semiconductor materials always outperform polycrystalline or amorphous thin films in yielding higher device power-conversion efficiency (PCE) because of the presence of much less defects in single crystals.[1] The key parameters of a semiconductor for solar-cell application include optical bandgap, absorption coefficient, carrier diffusion length, and so forth. For a given semiconductor, the carrier diffusion length determines how efficient the photogenerated free charges can be collected by the p−n junction and electrodes and, thus, limits the PCE of a solar cell. Organometal trihalide perovskite (OTP) solar cells use nature-abundant hybrid perovskite materials as active layers that can be deposited by versatile and low-cost approaches onto many different kinds of substrates with a scalable way. Despite the rapid increase of PCE of the OTP solar cells, one of the most fundamental properties that that enables these high PCEs has not been fully characterized, which is the carrier diffusion length.

> The carrier diffusion length measured in organometal trihalide perovskite is strongly dependent on material morphology.

The evolution in understanding the carrier diffusion length is illustrated in Figure 1. OTP solar cells started from amorphous or polycrystalline form of active layers in a mesoporous device structure that was inherited from the dye-sensitized solar cells (DSSC), in which the OTPs worked as sensitizers. This device structure, however, has not manifested the excellent electronic properties of the OTPs. In the first mesoporous structure OTP devices, the perovskite formed nanoparticles had size as small as

2−3 nm, and the absorption of sun light can be complete due to the very large surface area of the TiO_2 mesoporous electrode. A carrier or exciton diffusion length in the order of 1 nm is sufficient to extract the photogenerated excitons or free charges in the OTP layers to the mesoporous TiO_2 electrode.[2−5]

The breakthrough demonstration of planar heterojunction (PHJ) OTP devices indicated the OTP materials work as traditional semiconductors that should have much larger carrier mobility and recombination lifetime than insulating organic dyes.[6] In early efforts to understand why OTP materials work so well for both DSSC and PHJ structure solar cells, bipolar transport properties with a large diffusion length exceeding 100 nm in $CH_3NH_3PbI_3$ ($MAPbI_3$) polycrystalline thin films was revealed, which is much larger than all existing organic semiconductors.[7−11] Nevertheless, the films in these studies have qualities far worse than those used in the high efficiency devices. Like any semiconductor material, the carrier diffusion length in $MAPbI_3$ should be sensitive to presence of defects, such as film surfaces, grain boundaries and dislocations, and et al. Although the point defects in $MAPbI_3$ were found not form midgap deep-trap states,[12] a large density of charge traps have been observed at the grain boundaries and surfaces of the hybrid perovskite films.[13−15]

It was quickly realized by us and other groups that the size and crystallinity of the OTP grains are crucial in determining the PCE of these devices.[16] In the period of 2013−2014, most of the reported high-efficiency perovskite solar cells have a thickness around 300 nm. It turns out this optimized thickness is most likely limited by the grain size of $MAPbI_3$ polycrystal-
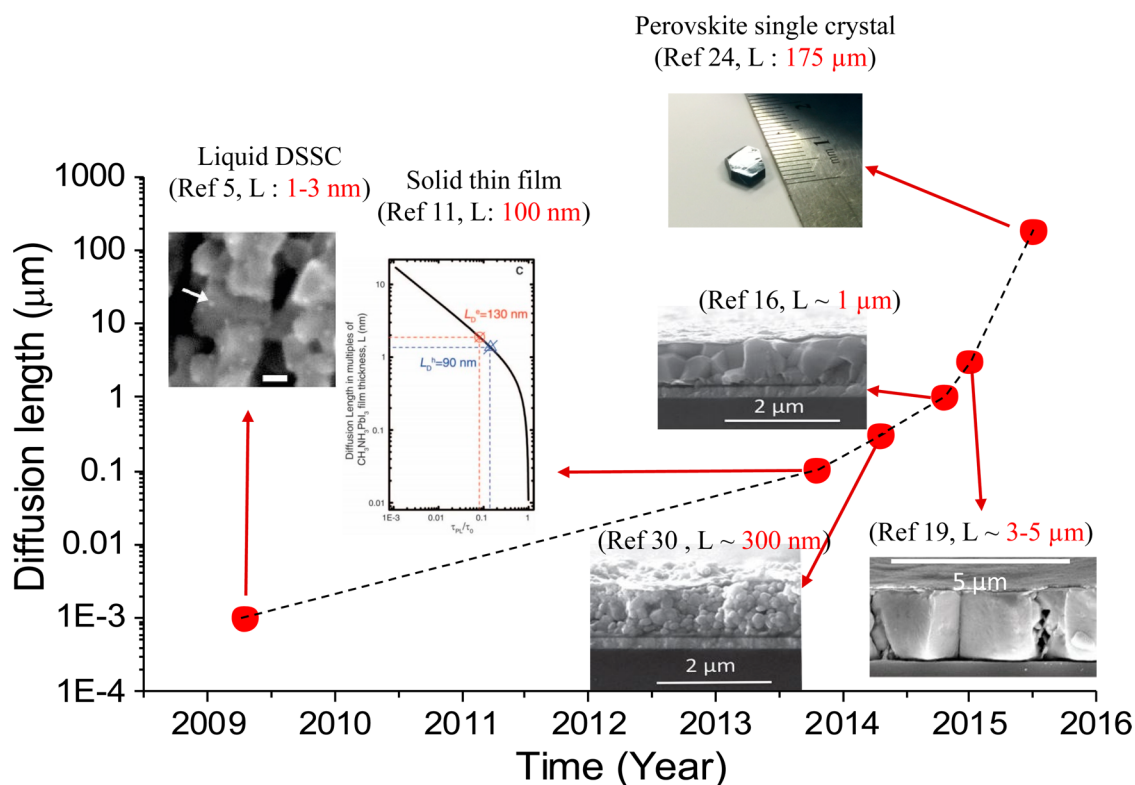
Figure 1. Evolution on the carrier diffusion length understanding. The typical material morphology or measured carrier diffusion length were shown. The first perovskite device with DSSC structure had a perovskite thickness of 1−3 nm. Reproduced from ref 5 with permission of ACS Publication, from refs 11 and 24 with permission of AAAS, from refs 16 and 30 with permission of John Wiley and Son, and from ref 19 with permission of the Royal Society of Chemistry (RSC).

line films formed by regular thermal annealing method.[17] However, thicker MAPbI$_3$ films are needed to enhance the absorption in the wavelength range close to the band edge.[16,18] Increasing annealing time for larger grain size is not a feasible approach because the hybrid perovskites turn to decompose overtime.[17] To address this issue, we used a solvent annealing process, that is, adding the comment solvent for the two precursors during thermal annealing process, to increase the OTP grain size to be comparable to the film thickness up to 1 μm.[16] The elimination of the grain boundaries in the carrier-transport direction reduced charge recombination by several times and increased the carrier diffusion length to above 1 μm. The internal quantum efficiency is close to 100% even in the 1 μm thick devices, whereas the depletion depth is around 100 nm. It was later demonstrated by us that the doctor-blade coated MAPbI$_3$ films have a carrier diffusion length which is comparable to film thickness of 3−5 μm, thanks to the formation of columnar structure grains, which connect the anode and cathode directly.[19]

A burning question that naturally arises is, "What is the limit of carrier diffusion length in this material, and does the carrier diffusion process limit the carrier extraction in working devices?" MAPbI$_3$ single crystals with a size close to or larger than the carrier diffusion length are thus needed so that we can use the simple device charge extraction efficiency measurement to determine the carrier diffusion length. The growth of the hybrid perovskite single crystals started more than 20 years ago by A. Poglitsch and D. Weber, and it is based on the condensation of concentrated aqueous solution of the precursor.[20] A common trick in synthesize MAPbI$_3$ single crystals is the temperature of the solution for crystal growth

needs to be above 40 °C to prevent the formation of translucent yellow crystals of $(CH_3NH_3)_4PbI_6 \cdot 2H_2O$.[21−23] This method generally yields small single crystals with size less than 1 mm with irregular shape because of the uncontrolled formation of too many seeds.

It is not until recent that large MAPbX$_3$ single crystals have been successfully synthesized via different methods.[23−26] Because the decomposition temperature of the hybrid perovskite materials is very low, the growth of single crystal hybrid perovskite materials are predominately solution based. We synthesized MAPbI$_3$ single crystals with sizes up to 10 mm from a supersaturated precursor solution using a top-seeded solution-growth (TSSG) method as shown in Figure 2a. The small temperature gradient between the bottom and the top of the solution induced sufficient convection to transport the material to the large MSCs, which provides a stable supersaturate solution and temperature gradient during the whole crystal growth process and enables a homogeneous crystal growth. This method has been shown by us later to grow large size MAPbBr$_3$, MAPbCl$_3$, and mixed halide single crystals such as MAPbBr$_x$Cl$_{3−x}$ and MAPbBr$_x$I$_{3−x}$. Rather than using precursor of PbI$_2$, Y. Dang et al. used Pb(CH3COOH)$_2 \cdot$ 3H$_2$O in hydroiodic acid (HI) to mix with MAI and were able to grow MAPbI$_3$ single crystals with a diameter of 10 mm from a supersaturated precursor solution by cooling down the hot solution from 65 to 40 °C (Figure 2b).[23] D. Shi et al. reported the growth of millimeter scale MAPbX$_3$ single crystal by an antisolvent vapor-assisted crystallization method (ASVSC).[25] Single MAPbX$_3$ crystals grew out of the solution when the MAPbX$_3$ precursor solutions were mixed with the orthogonal solvent, as shown in Figure 2c. A cubic shape MAPbBr$_3$ with
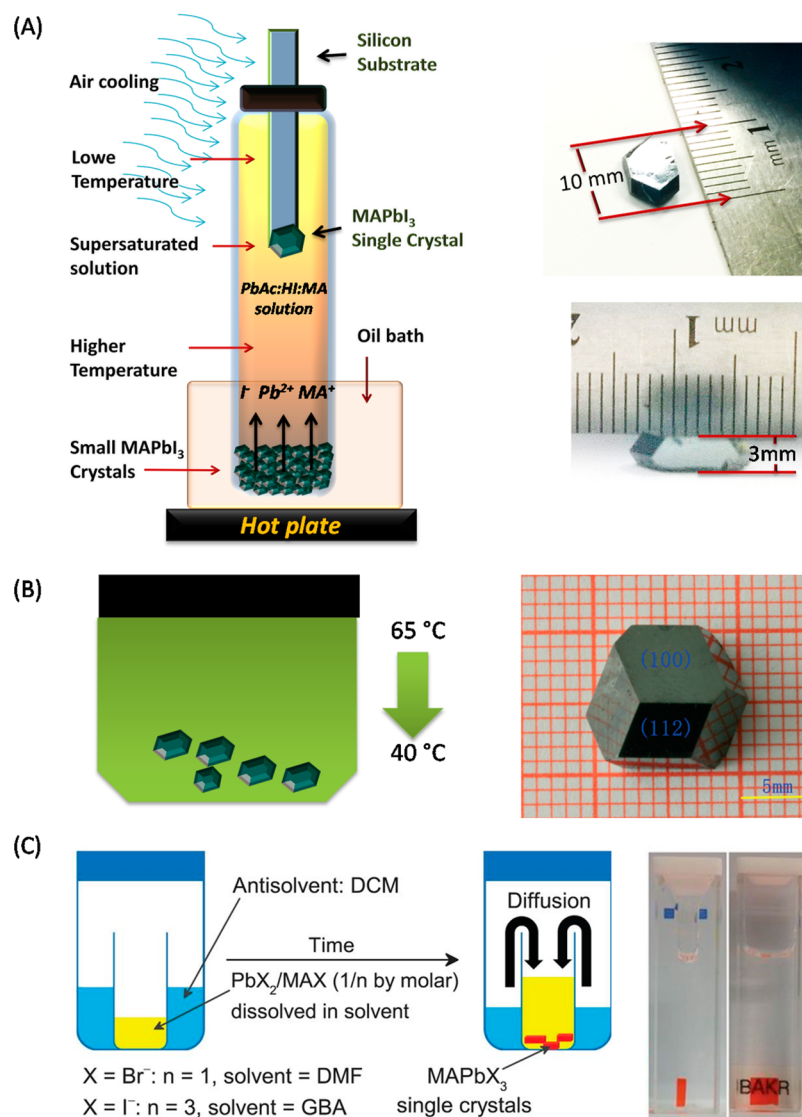
Figure 2. Methods to grow the large size single crystals and pictures of the single crystals. Reproduced from refs 24 and 25 with the permission of AAAS and from ref 23 with the permission of RSC.

millimeter scale size was achieved, whereas the MAPbI$_3$ crystals grown by this method showed smaller size and irregular shape, which may be caused by the much higher solubility of MAPbI$_3$ in the good mother solvent than MAPbBr$_3$. The solvothermal method based on inverse solubility has been applied to grow the mixed halide perovskite MAPb(Br$_{1-x}$Cl$_x$)$_3$.[27] Based on the observation of substantial decrease of MAPbX$_3$ solubility in certain solvents at elevated temperatures, Saidaminov et al. recently applied the solvothermal method to grow MAPbX$_3$ single crystals at a much quick rate than the ASCSC method.[26] It should be noted there is barely any study of the electronic property difference of the same type of perovskite single crystals grown by different methods. We speculate that different methods give rise to different quality of single crystals, similar to silicon crystals or wafers.

The grown high quality hybrid perovskite single crystals enabled the study of their intrinsic electronic properties. Two groups independently characterized the carrier diffusion length in MAPbI$_3$ single crystals (Figure 3)[24] and D. Shi et al. also reported the carrier diffusion length in MAPbBr$_3$ single crystals. The hole mobilities were reported to be 164 ± 25 cm^2/(V s)

and 2.5 cm^2/(V s) for the MAPbI$_3$ single crystals grown by the TSSG method (mobility measured by time-of-flight method) and ASVSC method (mobility measured by space-large-limited-current method), respectively. The mobility of MAPbBr$_3$ single crystals grown by ASVSC method reached 115 cm^2/(V s) (mobility measured by time-of-flight method). There is a large discrepancy in the reported charge recombination lifetime for the hybrid perovskite single crystals, whose possible explanation will be discussed later. The transient photoluminescence and absorption gives a lifetime in the range of 0.3 μs ∼ 1.2 μs for MAPbI$_3$ under high charge injection level, whereas transient photovoltage and impedance spectroscopy gave a much longer carrier recombination lifetime of 80 μs ∼ 100 μs under 1 sun illumination injection condition.[24] Due to the large difference in lifetime measurement results, the carrier diffusion length in MAPbI$_3$ and MAPbBr$_3$ single crystals and MAPbI$_3$ grown by ASVSC method were estimated to be 8 and 17 μm, respectively, whereas in TSSG grown MAPbI$_3$ single crystals have a very long carrier diffusion length of >175 μm. We fabricated the first single crystal perovskite solar cell using the 3 mm thick MAPbI$_3$ single crystals grown by the TSSG method.
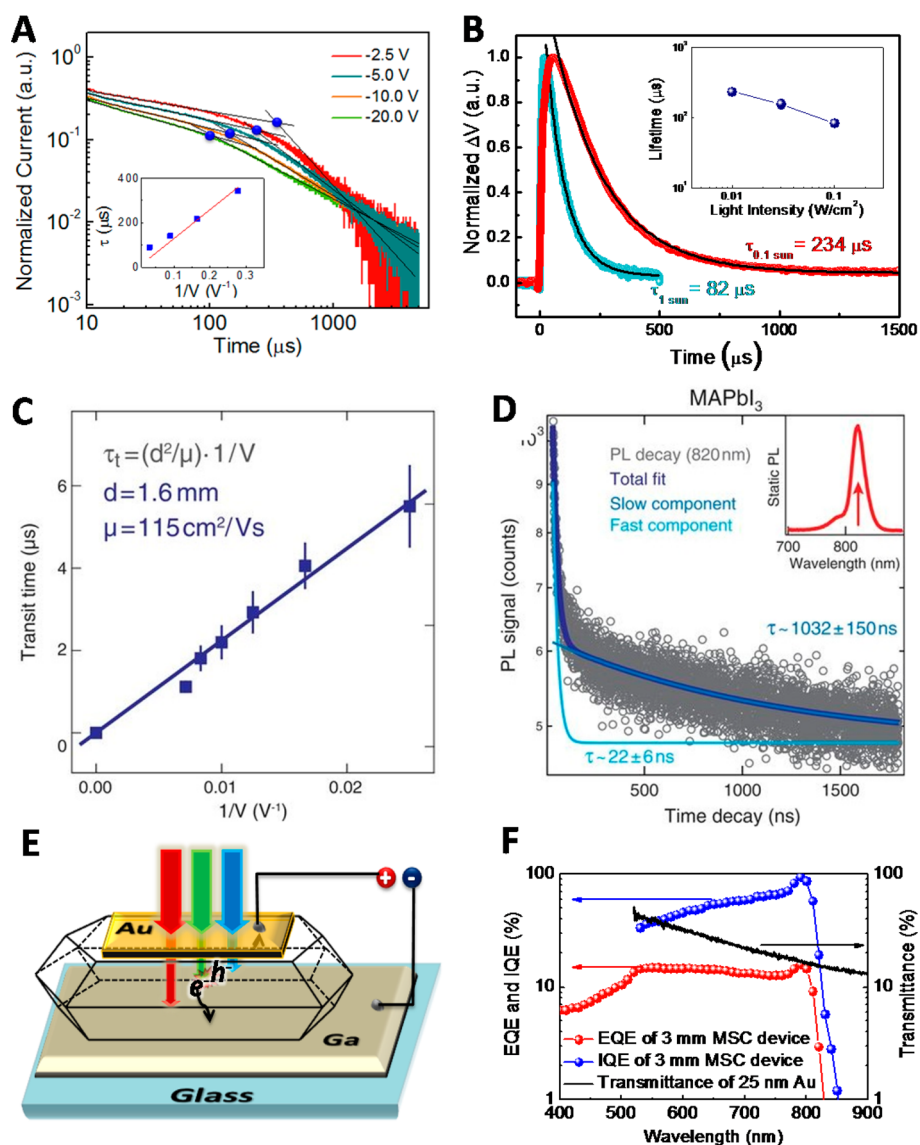
Figure 3. Carrier mobility (A, C) and recombination lifetime (B, D) measurement results. (E) Structure of the single crystal devices with Ga as cathode and Au as anode. (F) Absorption of Au electrode, external quantum efficiency (EQE) and internal quantum efficiency (IQE) of the single crystal devices. Reproduced from from ref 24 and 25 with permission of AAAS.

The devices have a simple structure with gallium as the cathode, and a semitransparent thin gold film as the anode (Figure 3e). The devices showed surprisingly a high internal quantum efficiency close to 100% under a very weak illumination (Figure 3f). This indicates the carrier diffusion length should be at least comparable to the crystal thickness, which is 3 mm in this case, so that charges photogenerated right underneath the semitransparent Au electrode can be efficiently collected by counter electrode. We also revealed the responsivity of the single crystal device (short-circuit current density versus incident-light intensity) is strongly dependent on light injection level, reconciling the large difference of carrier diffusion length under strong and weak light for the single crystals.

To accurately determine the carrier diffusion length, it is critical to accurately measure the carrier mobility and recombination lifetime because the product of them determines the carrier diffusion length. However, there is a wide range of carrier mobility and lifetime reported so far in the literature. For MAPbI$_3$, the carrier mobility measured by transistor character-

> There is a large variation in the measured carrier mobility and carrier recombination in hybrid perovskite, which is highly sensitive to material's morphologies and characterization methods.

ization, transient photocurrent (TPC), or time-of-flight (ToF), photoluminescence quenching, terahertz photoinduced transient absorption, Hall effect, and space-charge limited current (SCLC) yielded mobilities of 10^{-5} cm^2/(V s),[28] 0.001−0.005 cm^2/(V s),[16,29−31] 0.02−2 cm^2/(V s),[25,26] 8−30 cm^2/(V s),[32] 10−150 cm^2/(V s)[22,24,29,33] and 120−150 cm^2/(V s),[24,25] respectively. The discrepancy of carrier mobility can be reconciled by considering the measured different carrier transport processes by these techniques and morphologies of the materials under investigation. First, the extremely low field

effect carrier mobility can be explained by the failure of fabricating room-temperature operational hybrid perovskite transistors which is still an open challenge for the hybrid perovskite community. One possible reason is that the electromigration of ions in hybrid perovskites screen the gate field.[34] This also raises an issue for charge carrier mobility measurements, that is, the electromigration of ions needs to be excluded in the measurement of electric conductivity. In some cases, such as at above room temperature and small size grains in the perovskite films, the electromigration can dominate the total current.[35] Second, different electronic processes were measured by different techniques. Hall Effect and trap-filled SCLC measurements characterize the band transport behavior, whereas the TPC and ToF measurement are susceptible to charge traps because the charge trapping and detrapping process would slow down the charge extraction process and elongate the transit time. Thus, the mobility extracted from the TPC measurement can be much lower than the band transport mobility (or intrinsic mobility) of the perovskite materials. Nevertheless, it reflects the real charge extraction process under the practical device working condition, and thus it should be used to study the charge extraction process. The transient terahertz photoconductivity measurements should also give band-transport mobility because at such high frequency, the charge carriers can barely transport across the grain boundaries and go through the trapping and detrapping process. Hall mobility is expected to approach the TPC or time-of-flight mobility only if the trap band-tail states are negligible. We observed the coincidence of Hall mobility with ToF mobility in our MAPbI$_3$ single crystals, which provides another evidence for the presence of negligible bulk-traps in the MAPbI$_3$ single crystals.[24] Third, the mobility of the hybrid perovskite is sensitive to the material morphology. The presence of amorphous phase or grain boundaries inevitably reduces carrier transport mobility. This explains the large discrepancy of the carrier mobility measured by the same methods, for example, the over ten times' difference carrier mobilities measured by photoluminescence quenching.[25,26] We demonstrated that larger grain size by thermal annealing MAPbI$_3$ increased the Hall mobility from 12 cm^2/(V s) to over 30 cm^2/(V s),[17] and further the grain boundary passivation by PCBM on these thermal annealed MAPbI$_3$ films boosted the Hall mobility of polycrystalline thin film MAPbI$_3$ to 115 cm^2/(V s),[29] which is close to that of single crystalline MAPbI$_3$.[24] Fourth, the low mobility charge transport layers used in real perovskite devices can affect the accuracy of the carrier mobility characterization of the perovskite layer. Because the carrier mobilities in most organic semiconductors, which are used as charge transport layers in perovskite solar cells, is in the order of 10^{-4}–10^{-2} cm^2/(V s). The several orders magnitude smaller carrier mobility in the charge transport layer makes the measured transit time by TPC to be dominated by the charge transportation process in these organic charge transport layers. As a direct evidence for this speculation, the measured charge extraction time from TPC curves shown in Figure 4 is the same in the doctor-blade coated devices with a structure of ITO/PEDOT:PSS/MAPbI$_3$ (1.1–3.0 μm)/PCBM (20 nm)/C60(20 nm)/BCP (8 nm)/Al with varied MAPbI$_3$ thickness. Therefore, the measured carrier mobility and mobility increase might be underestimated by previous TPC measurement.[16,29] One needs to specify the measurement method, applied electric field, temperature, device and film geometry, and material morphology when presenting the measured carrier mobility of
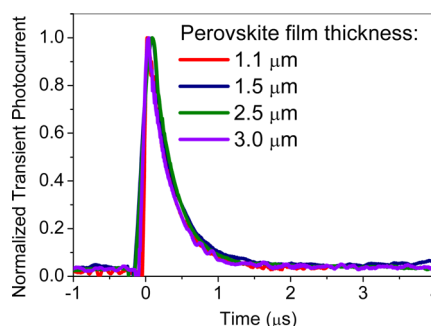

Figure 4. Time-of-flight measurement transient photocurrent curves of 1−3 μm thick polycrystal thin films formed by doctor-blade coating.

perovskite materials or perovskite devices. We expect the intrinsic carrier mobility of MAPbI$_3$ inside the grains to be close to that of MAPbI$_3$ single crystals[24,29] because the crystallinity of most MAPbI$_3$ polycrystalline films yielding a device power conversion efficiency above 15% is close to that of the single crystals.

For thin film solar cells, the charge recombination lifetime is one of the most important parameters for any device modeling and design. Comparing to carrier mobility measurement, the carrier recombination time measurement for hybrid perovskite materials is even less established. The general methods for minority carrier lifetime measurement in silicon include transient microwave-reflection photoconductive decay (μPCD), surface photovoltaic (SPV), and quasi-steady-state photoconductance decay measurements (QSSPD), whereas the minority carrier recombination lifetime measurement for hybrid perovskite materials inherited that of organic semiconductors using time-resolved photoluminescence (TRPL) and transient absorption (TA). The time constant measured by transient PL or absorption techniques should be the effective charge recombination lifetime (τ_{eff}), rather than the intrinsic or bulk charge recombination lifetime (τ_b) of the hybrid perovskites. The effective charge recombination lifetime is governed by both bulk charge recombination lifetime (τ_b), and surface charge recombination lifetime (τ_S):

$$\frac{1}{\tau_{eff}} = \frac{1}{\tau_b} + \frac{1}{\tau_S}$$

(1)

The surface charge recombination lifetime, or how fast the surface excess charge concentration decays, is determined by both surface charge recombination velocity and diffusion rate of free charges generated in the bulk toward the surface. A quick estimation of the diffusion time needed to travel a distance of 100 nm, which is the approximate light penetration length in transient spectroscopy study with 400 nm excitation light, is less than 10 ps. It is much faster than the charge recombination at the hybrid film surfaces, and thus, most of the measured recombination lifetime should be dominated by surface charge recombination rate. The bulk charge recombination is determined by the radiative (also known as band-to-band) charge recombination lifetime (τ_{rad}), Auger recombination lifetime (τ_A), and Shockley−Read−Hall (SRH) recombination via traps within the energy gap (τ_{SRH}). Both the bulk and surface charge recombination lifetime can be a strong function of the minority-carrier density (doping concentration) and excess carriers concentrations (injection level or light intensity), though these conditions were not specified in most of the

current reported carrier recombination lifetime measurement for the hybrid perovskite materials.

The effective recombination lifetime approaches the bulk recombination lifetime only if the surface of the perovskite materials is well passivated so that τ_S is much longer than τ_b. The perovskite single crystals grown by the solution processes inevitably have a relative large trap density on the surface because of the nonstoichiometric surface and possible damaging of the surface by the solvents, as evidenced by the smaller charge extraction efficiency for the shorter wavelength light than longer wavelength light in the single crystal devices.[24] Nevertheless, the surface traps can be effectively passivated even in polycrystalline films.[31] Our previous study demonstrate that there is a large density of surface traps caused by the easy surface decomposition of MAPbI$_3$, whereas the surface traps can be partially passivated by fullerene attachment,[29] and similar passivation effect was also observed using pyridine treatment.[36,37] Further study of single crystal surface defect and passivation effect is urgently needed to have a better idea on the intrinsic charge recombination lifetime and how does the defect impact it.

> After demonstration of the superior electronic properties of perovskite single crystals for photovoltaic application the next question naturally arises is whether the perovskite single crystals can or should be a next wave of material for high efficiency perovskite solar cells.

One interesting phenomenon is the appearance of strong below-bandgap absorption for the single crystals, which has not been observed by polycrystalline thin films. For example, the absorption edge and external quantum efficiency cutoff of a MAPbI$_3$ single crystal is extended to 850 nm, compared to the 800 nm absorption edge for polycrystalline thin films (Figure 5). The red-shifted of the absorption edge by 50 nm could potentially increase the upper limit of short circuit current density (J_{SC}) in MAPbI$_3$-based solar cells from 27.5 mA cm^{-2} to 33.0 mA cm^{-2} by using the perovskite single crystals.[24] Nevertheless, the application of much thicker single crystals increases the material usage, and may cause the loss of device open circuit voltage (V_{OC}) and fill factor (FF) because the

charge bulk recombination chance also increases with increasing active layer thickness. Therefore, direct application of very THICK single crystals for enhanced absorption might not bring significant advantages in terms of cost and energy conversion efficiency.

On the other hand, the complete absence of grain boundaries in the single crystals is expected to reduce the charge recombination at the grain boundaries, which can increase the device V_{OC} and FF. To this end, the application of THIN perovskite single crystal wafer, or even large grain size multicrystals, should enhance the device efficiency. Nevertheless, there is no method yet to grow thin perovskite single crystals at wafer scale, the alternative material large aspect ratio perovskite multicrystals is thus pursued. Because a perovskite film thickness below 1 μm is thick enough to absorb most of incident light above its bandgap, a straightforward solution to reduce the total grain boundary area is to increase the grain lateral size. We did a simulation to predict the impact of grain size on the PCE of the perovskite solar cells according to the basic idea that defects at grain boundary and surface would reduce recombination lifetime. We computed how the increase recombination at surface and grain boundary increase dark current and, thus, decrease V_{OC} and FF. Then, the device PCE versus grain size was derived. The details of the simulation can be seen in the Computational Methods section. We also considered different charge recombination center densities in our simulation, which is closely related to the surface trap density and degree of surface/grain boundary passivation.

Figure 6 show the calculated device efficiencies based on MAPbI$_3$ polycrystalline films with and without surface passivation as a function of grain size. The simulation results emphasize the importance of surface/grain boundary passivation, in addition to the large grain size. The general trend is that large grain size gives to higher device PCE; however, the PCE saturates to around 16% if the top and bottom surfaces are not well passivated (blue dashed line). A better passivation of top and bottom surface can increase the device efficiency up to 20% with a grain size of 10 μm (red dashed lines). However, if the surface and grain boundary defect density is very small (or well passivated), a much higher device PCE of 24–25% can be achieved with a grain size of 10 μm (solid lines), and surface passivation is still important to achieve this highest efficiency.

An initial experiment study of the grain size dependent perovskite solar cell PCE was conducted by Nie et al. who changed the grain size by varying the temperature of casting solution.[38] An obvious correlation was observed between the device J_{SC} with grain size, but not between device V_{OC} with
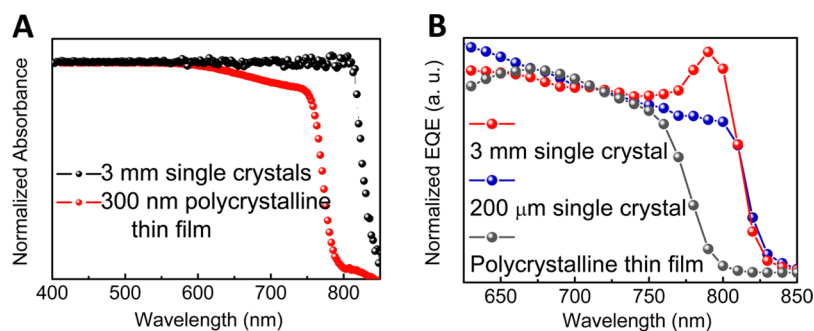
Figure 5. Normalized absorption (a) and external quantum efficiency spectra (b) of the 3 mm thick and 200 μm thick single crystals, and a 300 nm polycrystalline thin film based devices. Reproduced from ref 24 with permission of AAAS.
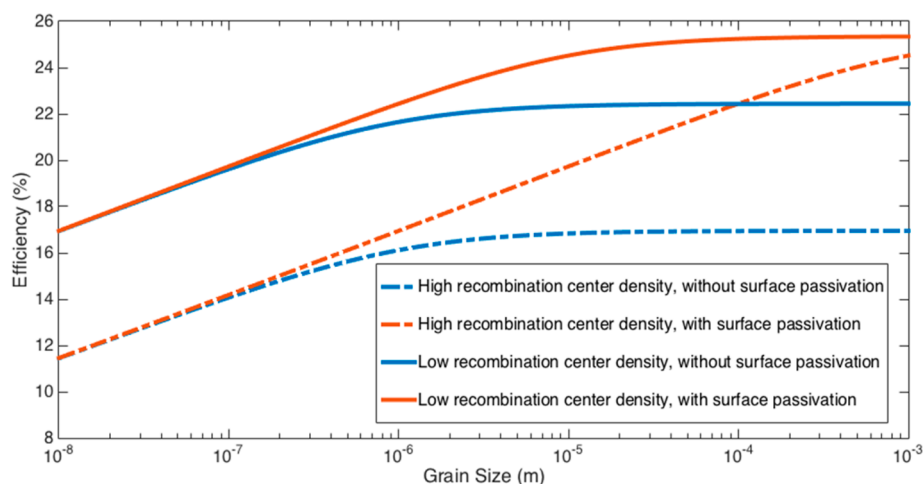
Figure 6. Device efficiency simulation result of perovskite solar cells as a function of grain size and surface passivation. The solid lines present the efficiency of the devices with very low recombination center density at the grain boundary and surface. The dashed lines present the devices with low quality and high recombination center density at the grain boundary and surface. The surface passivation refers the reduction of charge recombination centers at the perovskite/cathode and perovskite/anode interfaces.

grain size. This might be caused by the fact that the other material parameters, such as composition, doping, surface defects, and so forth, varied as well with respect to the casting-solution temperature, in addition to the grain size. Another possible explanation is that the "millimeter-size" grains might not be really single-crystalline. We and several other group observed the millimeter-size "domain" formation by doctor-blade coating or hot-solution casting, whereas the cross-section scanning electron microscopy images indicate the films were polycrystalline.[19] This will need to be further studied until a consensus can be reached.

On the basis of the simulation result in Figure 6, passivating the charge traps at the grain boundaries to reduce charge recombination can relieve the requirement for very large size perovskite multicrystals. Our previous study revealed that fullerene passivated hybrid perovskite polycrystalline films have 3−4 times longer carrier recombination lifetime. Nevertheless, there is still significant grain boundary charge recombination in the films grown by solvent-annealing assisted interdiffusion method, which is several times quicker than bulk charge recombination.[29] Recently, we were able to dramatically suppress the total charge recombination at grain boundary in polycrystalline perovskite solar cells by increasing the grain lateral size/thickness aspect ratio. We found that using nonwetting hole transport layer covered ITO substrates could effectively increase the grain aspect ratio from 100% to 800%.[31] The suppressed nucleation by the nonwetting hydrophobic HTLs reduced the total nuclei density, and the nonwetting smooth HTL surface also facilitated the grain boundary migration during grain ripening process, which induces the formation of the large aspect-ratio grains. The thermal admittance spectroscopy study confirmed the >10 times reduction of active charge traps originated from grain boundary area reduction. The dramatically suppressed grain boundary recombination increased the device J_{SC} and V_{OC} simultaneously and boosted the PCE to 19.3%.[31] Nevertheless, there is still large room for the device PCE enhancement in terms of surface passivation. TPV revealed that the large aspect ratio grains with all-round passivated grains have carrier recombination lifetime approaching to that of single crystals at zero bias, however the charge recombination increased strongly with bias approaching

to V_{OC}. This indicates the field charge recombination dependent carrier dynamics should be investigated in the future.

> Perovskite single crystals can be an ideal platform for the study of unique physical and chemical properties. Perovskite single crystals may be first commercialized in applications other than photovoltaics.

It is too early to predict whether the perovskite single crystals will be the materials in the commercial perovskite solar cells, in viewing of the polycrystalline perovskite films already produce solar cells with high efficiency of around 20%. Nevertheless, the single crystals perovskite provided an excellent platform to understand the intriguing fundamental properties of hybrid perovskites because of the simplicity provided in design experiment and analysis results. One example is that the different facets of the crystals allow easy study of grain orientation dependent electronic properties. The initial study of carrier diffusion length in perovskite single crystals assigned the very low trap density in single crystals to the origin of long carrier diffusion length. Nevertheless, other effects, such as phonon scattering, dipole alignment of MA$^+$ ions, and so forth, have not been examined yet, which might also contribute to the long carrier diffusion length. We expect more studies will be conducted in these directions in the future, which will help understanding the fundamental intrinsic properties of hybrid perovskites and designing of new materials for better stability and environmental sustainability.

The excellent electronic properties of hybrid perovskite singe crystals can enable other applications. The very large carrier mobility and carrier recombination lifetime make the hybrid perovskite material an ideal candidate for ionization radiation detectors. In addition, the hybrid perovskites have the second heaviest stable element-Pb, which brings a strong stopping power of this material to X-ray and γ ray. We first evaluated the

application of the single-crystalline MAPbI$_3$ for γ-ray detection and energy harvesting.[24] The nonoptimized simple device with a structure of Ga/MAPbI$_3$/Au showed a γ-ray detection efficiency close to 4%, measured with an intense cesium-137 source.[24] Application of polycrystalline thin film MAPbI$_3$ for soft X-ray detection was also attempted by Yakunin et al, yielding a X-ray sensitivity up to 25 μC mGy$_{air}^{-1}$ cm^{-3}, which is competitive to the best amorphous Se X-ray detectors.[39] However, its relatively low mobility-lifetime products of the polycrystalline film still limits its application for hard X-ray detection, where a much thicker perovskite layer is needed to stop X-ray. Finally, because low threshold optical excitation laser and high gain, low noise photodetectors have also been demonstrated using polycrystalline perovskite films and nano-crystals.[40−44] The application of the single crystalline material is expected to further broaden its applications in these areas for higher performance due to the much better electronic properties.

COMPUTATIONAL METHODS

Device Efficiency Simulation. The defects and imperfections at grain boundaries and surfaces can act as recombination centers for charges and, thus, affect the recombination lifetime as

$$\tau_{eff} = (\sigma v N_{sr})^{-1} \tag{2}$$

where τ_{eff} is the effective recombination lifetime, σ is the capture cross section, v is the thermal velocity of the carriers, and N_{sr} is the effective density of recombination centers (cm^{-3}). One of the most attractive features of perovskites is their ability to form very good polycrystals through low temperature solution processes. Thus, the density of bulk crystal defects in perovskite materials can be negligible comparing to that at the grain boundaries and surfaces. Assuming grain boundaries and surfaces have the same concentration of recombination centers per unit area N_{ss} and grains with the size of d meter square, we can derive N_{sr} in perovskite thin films with different grain size and different passivation conditions. Without surface passivation

$$N_{sr} = \frac{d+t}{dt} N_{ss} \tag{3}$$

After surface passivation

$$N_{sr} = \frac{1}{d} N_{ss} \tag{4}$$

where t is the thin film thickness (= 500 nm in our calculation). Substituting eq 3 and 4 into 2, the τ_{eff} without passivation can be given as

$$\tau_{eff} = (\sigma v N_{ss})^{-1} \times \frac{dt}{d+t} \tag{5}$$

the τ_{eff} with passivation can be given as

$$\tau_{eff} = (\sigma v N_{ss})^{-1} \times d \tag{6}$$

Thus, the value of $(\sigma v N_{ss})^{-1} = k_1$ can act as one indicator of the quality of the thin film including the composition and crystallization. The lower the recombination center density, the higher k_1 will be. Then the dark current characteristics are given as

$$J_{dark} = J_{od}[\exp(\lambda_d V - 1)] + J_{or}[\exp(\lambda_r V - 1)] \tag{7}$$

in which $\lambda_d = q/n_d kT$, $\lambda_r = q/n_r kT$. J_{od} presents the diffusion induced reverse saturation current = $(qD_p p_{n0}/L_p) + (qD_n n_{p0}/L_n)$ and $n_d = 1$; J_{or} presents the recombination induced reverse saturation current = $q n_i W/2\tau_{eff}$ and $n_r = 2$; where D_p and D_n are diffusion coefficient for electron and hole; L_p and L_n are diffusion length for electron and hole; W is the depletion width extracted from Mott−Schottky plot of the capacitance−voltage measurement. Then the open-circuit voltage (V_{OC}) is given by the relation

$$V_{OC} \approx \frac{nkT}{q} \ln\left(\frac{J_{SC}}{J_0}\right) \tag{8}$$

where n is the ideality factor for the diode property depending on recombination dynamics in the devices. During the calculation, we assumed a fixed short circuit current $J_{SC} = 24$ mA cm^{-2} because the diffusion length usually comparable or larger than the thin film thickness in the well-optimized perovskite solar cells. The fill factor (FF) is given by

$$FF = \frac{v_{OC} - \ln(v_{OC} + 0.72)}{v_{OC} + 1} \tag{9}$$

where v_{OC} is defined as the normalized V_{OC}: $v_{OC} = qV_{OC}/nkT$.

AUTHOR INFORMATION

Corresponding Author

*E-mail: jhuang2@unl.edu.

Notes

The authors declare no competing financial interest.

Biographies

Prof. Jinsong Huang received his Ph.D. degree in Material Science and Engineering from the University of California—Los Angeles in 2007. He is now the Susan J. Rosowski Associate Professor in the Department of Mechanical Engineering at University of Nebraska—Lincoln (UNL). His current research interests include solution processed electronic materials for applications in sensing, energy and consumer electronics. More information can be found at www.huanggroup.unl.edu.

Mr. Yuchuan Shao received his B.S. degree from University of Science and Technology of China and his M.S. degree from Shanghai Institute of Optics and Fine Mechanics. Thereafter, he joined Prof. Huang's group as a Ph.D. student. His research interests include engineering and physics of perovskite solar cells.

Dr. Qingfeng Dong received his B.S. degree in Chemistry and Ph.D. degree in Polymer Chemistry and Physics from Jilin University. He is currently a postdoctoral research associate at University of Nebraska—Lincoln. His research focuses on perovskite solar cells.

ACKNOWLEDGMENTS

REFERENCES

(1) Luque, A.; Hegedus *Photovoltaic Science and Engineering*; S. John Wiley and Sons: Chichester, England, 2003.

(2) Lee, M. M.; Teuscher, J.; Miyasaka, T.; Murakami, T. N.; Snaith, H. J. Efficient hybrid solar cells based on meso-superstructured organometal halide perovskites. *Science* 2012, 338, 643−647.

(3) Im, J. H.; Jang, I. H.; Pellet, N.; Gratzel, M.; Park, N. G. Growth of CH$_3$NH$_3$PbI$_3$ cuboids with controlled size for high-efficiency perovskite solar cells. *Nat. Nanotechnol.* 2014, 9, 927−932.

(4) Burschka, J.; Pellet, N.; Moon, S. J.; Humphry-Baker, R.; Gao, P.; Nazeeruddin, M. K.; Gratzel, M. Sequential deposition as a route to high-performance perovskite-sensitized solar cells. *Nature* **2013**, *499*, 316−319.

(5) Kojima, A.; Teshima, K.; Shirai, Y.; Miyasaka, T. Organometal halide perovskites as visible-light sensitizers for photovoltaic cells. *J. Am. Chem. Soc.* **2009**, *131*, 6050−6051.

(6) Liu, M.; Johnston, M. B.; Snaith, H. J. Efficient planar heterojunction perovskite solar cells by vapour deposition. *Nature* **2013**, *501*, 395−398.

(7) Stranks, S. D.; Eperon, G. E.; Grancini, G.; Menelaou, C.; Alcocer, M. J. P.; Leijtens, T.; Herz, L. M.; Petrozza, A.; Snaith, H. J. Electron-hole diffusion lengths exceeding 1 micrometer in an organometal trihalide perovskite absorber. *Science* **2013**, *342*, 341−344.

(8) Xiao, Z. G.; Dong, Q. F.; Bi, C.; Shao, Y. C.; Yuan, Y. B.; Huang, J. S. Solvent Annealing of Perovskite-Induced Crystal Growth for Photovoltaic-Device Efficiency Enhancement. *Adv. Mater.* **2014**, *26*, 6503−6509.

(9) Wang, Q.; Shao, Y. C.; Dong, Q. F.; Xiao, Z. G.; Yuan, Y. B.; Huang, J. S. Large fill-factor bilayer iodine perovskite solar cells fabricated by a low-temperature solution-process. *Energy Environ. Sci.* **2014**, *7*, 2359−2365.

(10) Liang, P. W.; Liao, C. Y.; Chueh, C. C.; Zuo, F.; Williams, S. T.; Xin, X. K.; Lin, J. J.; Jen, A. K. Y. Additive enhanced crystallization of solution-processed perovskite for highly efficient planar-heterojunction solar cells. *Adv. Mater.* **2014**, *26*, 3748−3754.

(11) Xing, G. C.; Mathews, N.; Sun, S. Y.; Lim, S. S.; Lam, Y. M.; Gratzel, M.; Mhaisalkar, S.; Sum, T. C. Long-range balanced electron- and hole-transport lengths in organic-inorganic $CH_3NH_3PbI_3$. *Science* **2013**, *342*, 344−347.

(12) Kim, J.; Lee, S.-H.; Lee, J. H.; Hong, K.-H. The role of intrinsic defects in methylammonium lead iodide perovskite. *J. Phys. Chem. Lett.* **2014**, *5*, 1312−1317.

(13) Noel, N. K.; Abate, A.; Stranks, S. D.; Parrott, E.; Burlakov, V.; Goriely, A.; Snaith, H. J. Enhanced photoluminescence and solar cell performance via Lewis base passivation of organic−inorganic lead halide perovskites. *ACS Nano* **2014**, *8*, 9815−9821.

(14) Shkrob, I. A.; Marin, T. W. Charge trapping in photovoltaically active perovskites and related halogenoplumbate compounds. *J. Phys. Chem. Lett.* **2014**, *5*, 1066−1071.

(15) Sanchez, R. S.; Gonzalez-Pedro, V.; Lee, J.-W.; Park, N.-G.; Kang, Y. S.; Mora-Sero, I.; Bisquert, J. Slow dynamic processes in lead halide perovskite solar cells. Characteristic times and hysteresis. *J. Phys. Chem. Lett.* **2014**, *5*, 2357−2363.

(16) Xiao, Z.; Dong, Q.; Bi, C.; Shao, Y.; Yuan, Y.; Huang, J. Solvent Annealing of Perovskite-Induced Crystal Growth for Photovoltaic-Device Efficiency Enhancement. *Adv. Mater.* **2014**, *26*, 6503−6509.

(17) Bi, C.; Shao, Y.; Yuan, Y.; Xiao, Z.; Wang, C.; Gao, Y.; Huang, J. Understanding the formation and evolution of interdiffusion grown organolead halide perovskite thin films by thermal annealing. *J. Mater. Chem. A* **2014**, *2*, 18508−18514.

(18) Yang, W. S.; Noh, J. H.; Jeon, N. J.; Kim, Y. C.; Ryu, S.; Seo, J.; Seok, S. I. High-performance photovoltaic perovskite layers fabricated through intramolecular exchange. *Science* **2015**, *348*, 1234−1237.

(19) Deng, Y.; Peng, E.; Shao, Y.; Xiao, Z.; Dong, Q.; Huang, J. Scalable fabrication of efficient organolead trihalide perovskite solar cells with doctor-bladed active layers. *Energy Environ. Sci.* **2015**, *8*, 1544−1550.

(20) Poglitsch, A.; Weber, D. Dynamic disorder in methylammoniumtrihalogenoplumbates (II) observed by millimeter-wave spectroscopy. *J. Chem. Phys.* **1987**, *87*, 6373−6378.

(21) Baikie, T.; Fang, Y.; Kadro, J. M.; Schreyer, M.; Wei, F.; Mhaisalkar, S. G.; Graetzel, M.; White, T. J. Synthesis and crystal chemistry of the hybrid perovskite (CH_3NH_3) PbI_3 for solid-state sensitised solar cell applications. *J. Mater. Chem. A* **2013**, *1*, 5628−5641.

(22) Stoumpos, C. C.; Malliakas, C. D.; Kanatzidis, M. G. Semiconducting tin and lead iodide perovskites with organic cations: phase transitions, high mobilities, and near-infrared photoluminescent properties. *Inorg. Chem.* **2013**, *52*, 9019−9038.

(23) Dang, Y.; Liu, Y.; Sun, Y.; Yuan, D.; Liu, X.; Lu, W.; Liu, G.; Xia, H.; Tao, X. Bulk crystal growth of hybrid perovskite material $CH_3NH_3PbI_3$. *CrystEngComm* **2015**, *17*, 665−670.

(24) Dong, Q.; Fang, Y.; Shao, Y.; Mulligan, P.; Qiu, J.; Cao, L.; Huang, J. Electron-hole diffusion lengths> 175 μm in solution-grown $CH_3NH_3PbI_3$ single crystals. *Science* **2015**, *347*, 967−970.

(25) Shi, D.; Adinolfi, V.; Comin, R.; Yuan, M.; Alarousu.; et al. Low trap-state density and long carrier diffusion in organolead trihalide perovskite single crystals. *Science* **2015**, *347*, 519−522.

(26) Saidaminov, M. I.; Abdelhady, A. L.; Murali, B.; Alarousu, E.; Burlakov, V. M.; Peng, W.; Dursun, I.; Wang, L.; He, Y.; Maculan, G.; et al. High-quality bulk hybrid perovskite single crystals within minutes by inverse temperature crystallization. *Nat. Commun.* **2015**, *6*, 7586.

(27) Zhang, T.; Yang, M.; Benson, E. E.; Li, Z.; van de Lagemaat, J.; Luther, J. M.; Yan, Y.; Zhu, K.; Zhao, Y. A facile solvothermal growth of single crystal mixed halide perovskite $CH_3NH_3Pb(Br_{1−x}Cl_x)_3$. *Chem. Commun.* **2015**, *51*, 7820−7823.

(28) Heo, J. H.; Im, S. H.; Noh, J. H.; Mandal, T. N.; Lim, C.-S.; Chang, J. A.; Lee, Y. H.; Kim, H.-j.; Sarkar, A.; Nazeeruddin, M. K. Efficient inorganic-organic hybrid heterojunction solar cells containing perovskite compound and polymeric hole conductors. *Nat. Photonics* **2013**, *7*, 486−489.

(29) Shao, Y.; Xiao, Z.; Bi, C.; Yuan, Y.; Huang, J. Origin and elimination of photocurrent hysteresis by fullerene passivation in $CH_3NH_3PbI_3$ planar heterojunction solar cells. *Nat. Commun.* **2014**, *5*, 5784.

(30) Xiao, Z.; Bi, C.; Shao, Y.; Dong, Q.; Wang, Q.; Yuan, Y.; Wang, C.; Gao, Y.; Huang, J. Efficient, high yield perovskite photovoltaic devices grown by interdiffusion of solution-processed precursor stacking layers. *Energy Environ. Sci.* **2014**, *7*, 2619−2623.

(31) Bi, C.; Dong, Q.; Shao, Y.; Wang, Q.; Yuan, Y.; Xiao, Z.; Huang, J. Non-wetting surface-driven high-aspect-ratio crystalline grain growth for efficient hybrid perovskite solar cells. *Nat. Commun.* **2015**, *6*, 7747.

(32) Wehrenfennig, C.; Eperon, G. E.; Johnston, M. B.; Snaith, H. J.; Herz, L. M. High charge carrier mobilities and lifetimes in organolead trihalide perovskites. *Adv. Mater.* **2014**, *26*, 1584−1589.

(33) Wang, Q.; Liu, X.; Shao, Y.; Gao, Y.; Huang, J. Qualifying composition dependent p and n self-doping in $CH_3NH_3PbI_3$. *Appl. Phys. Lett.* **2014**, *105*, 163508.

(34) Chin, X. Y.; Cortecchia, D.; Yin, J.; Bruno, A. Lead iodide perovskite light-emitting field-effect transistor. *Nat. Commun.* **2015**, *6*, 7383.

(35) Yuan, Y.; Chae, J.; Shao, Y.; Wang, Q.; Xiao, Z.; Centrone, A.; Huang, J. Photovoltaic Switching Mechanism in Lateral Structure Hybrid Perovskite Solar Cells. *Adv. Energy Mater.* **2015**, n/a.

(36) Vorpahl, S. M.; Stranks, S. D.; Nagaoka, H.; Eperon, G. E.; Ziffer, M. E.; Snaith, H. J.; Ginger, D. S. Impact of microstructure on local carrier lifetime in perovskite solar cells. *Science* **2015**, *348*, 683−686.

(37) Noel, N. K.; Abate, A.; Stranks, S. D.; Parrott, E. S.; Burlakov, V. M.; Goriely, A.; Snaith, H. J. Enhanced photoluminescence and solar cell performance via Lewis base passivation of organic−inorganic lead halide perovskites. *ACS Nano* **2014**, *8*, 9815−9821.

(38) Nie, W.; Tsai, H.; Asadpour, R.; Blancon, J.-C.; Neukirch, A. J.; Gupta, G.; Crochet, J. J.; Chhowalla, M.; Tretiak, S.; Alam, M. A. High-efficiency solution-processed perovskite solar cells with millimeter-scale grains. *Science* **2015**, *347*, 522−525.

(39) Yakunin, S.; Sytnyk, M.; Kriegner, D.; Shrestha, S.; Richter, M.; Matt, G. J.; Azimi, H.; Brabec, C. J.; Stangl, J.; Kovalenko, M. V.; Heiss, W. Detection of X-ray photons by solution-processed lead halide perovskites. *Nat. Photonics* **2015**, *9*, 444−449.

(40) Zhu, H.; Fu, Y.; Meng, F.; Wu, X.; Gong, Z.; Ding, Q.; Gustafsson, M. V.; Trinh, M. T.; Jin, S.; Zhu, X. Lead halide perovskite nanowire lasers with low lasing thresholds and high quality factors. *Nat. Mater.* **2015**, *14*, 636−642.

(41) Xing, G.; Mathews, N.; Lim, S. S.; Yantara, N.; Liu, X.; Sabba, D.; Grätzel, M.; Mhaisalkar, S.; Sum, T. C. Low-temperature solution-

processed wavelength-tunable perovskites for lasing. *Nat. Mater.* **2014**, *13*, 476−480.

(42) Dong, R.; Fang, Y.; Chae, J.; Dai, J.; Xiao, Z.; Dong, Q.; Yuan, Y.; Centrone, A.; Zeng, X.; Huang, J. High-Gain and Low-Driving-Voltage Photodetectors Based on Organolead Triiodide Perovskites. *Adv. Mater.* **2015**, *27*, 1912−1918.

(43) Fang, Y.; Huang, J. Resolving Weak Light of Sub-picowatt per Square Centimeter by Hybrid Perovskite Photodetectors Enabled by Noise Reduction. *Adv. Mater.* **2015**, *27*, 2804−2810.

(44) Lin, Q.; Armin, A.; Lyons, D. M.; Burn, P. L.; Meredith, P. Low Noise, IR-Blind Organohalide Perovskite Photodiodes for Visible Light Detection and Imaging. *Adv. Mater.* **2015**, *27*, 2060−2064.